Supplemental Figures

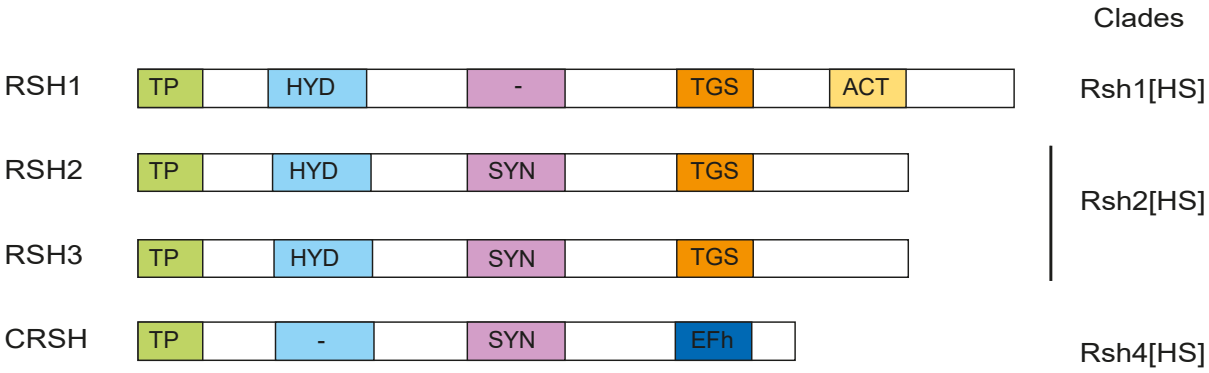

Supplemental Figure 1. Arabidopsis RSH domain structure.
Schematic representation of the domain structure of the Arabidopsis RSH enzymes, adapted from Atkinson et al., 2011. Membership of *RSH* gene clades is indicated to the right using the nomenclature of Atkinson et al., 2011. TP, chloroplast target peptide; HYD, ppGpp hydrolase domain; SYN, ppGpp synthase domain; TGS, TGS regulatory domain; ACT, ACT regulatory domain; EFh, calcium binding EF hand. RSH1 has a serine substitution in the ppGpp synthase domain that abolishes ppGpp synthase activity and the hydrolase domain of CRSH is degraded and may not be functional (Mizusawa et al., 2008, Atkinson et al., 2011).

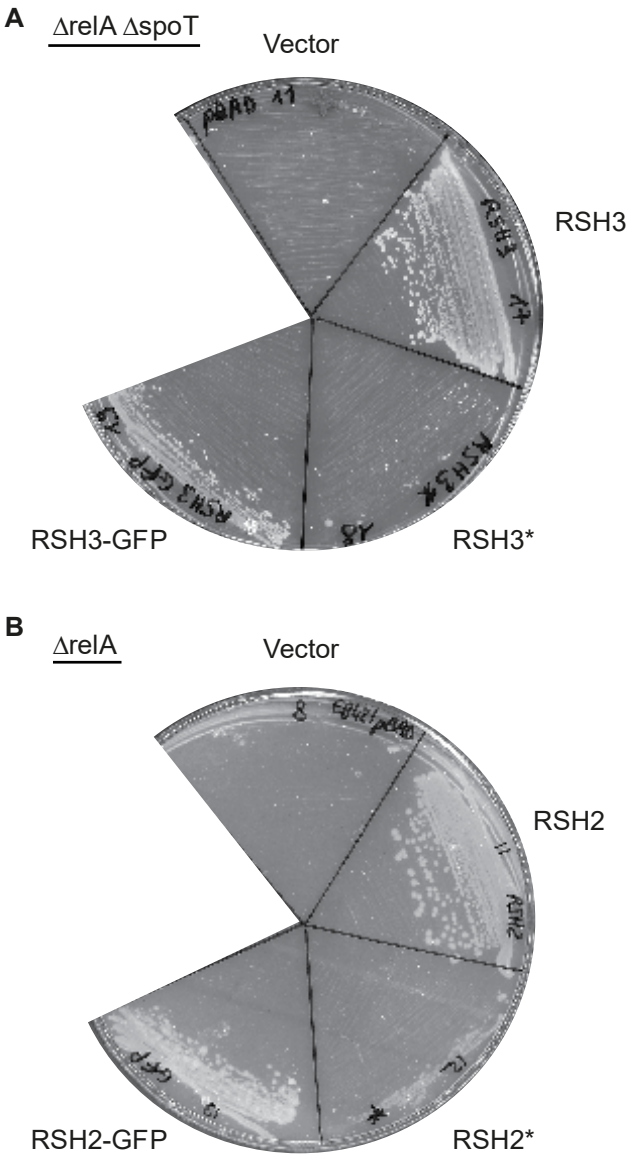

Supplemental Figure 2. Complementation of ppGpp deficient *E. coli* mutants by the expression of RSH2 and RSH3 GFP fusion proteins. (**A**) Expression of the mature form of RSH3 or an RSH3 GFP fusion complemented the growth of a ppGpp null (ΔrelA ΔspoT) mutant on minimal media without amino acids. Mutation of the ppGpp synthase active site abolished complementation (RSH3*). Bacteria containing the active RSH2 expression constructs could not be recovered in the ppGpp null mutant, as previously described (Mizusawa et al., 2008). Therefore RSH2 was tested in a ppGpp deficient relA mutant (ΔrelA) on SMG medium (**B**). Expression of the mature form of RSH2 and an RSH2 GFP fusion complemented ΔrelA, and mutation of the ppGpp synthase active site abolished complementation (RSH2*). In both cases the same GFP fusions were used as those in the OX:RSH2-GFP and OX:RSH3-GFP plant lines.

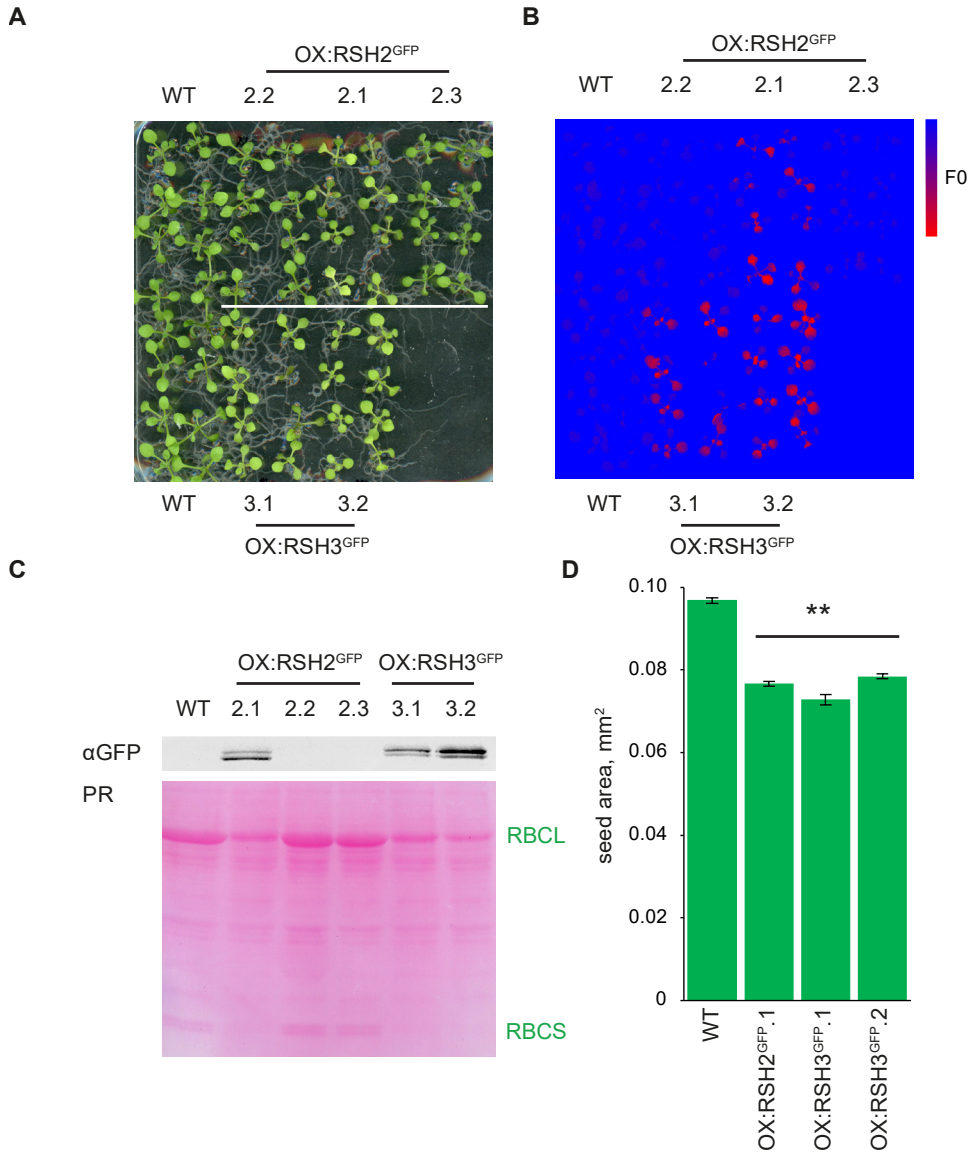

Supplemental Figure 3. Phenotypes of different RSH2-GFP and RSH3-GFP overexpression lines. Wildtype seedlings and different RSH2-GFP (OX:RSH2^{GFP}) and RSH3-GFP (OX:RSH3^{GFP}) overexpression lines were grown in plates for 12 DAS and (**A**) photographed and (**B**) imaged for chlorophyll fluorescence. F0 false color scale bar, 50-350 arbitrary units. (**C**) Immunoblots on equal quantities of total protein extracted from the same seedlings showed that the RSH-GFP fusion protein could be detected in the lines that were small and pale, had a high F0, and a low PSII maximum quantum yield QY. Proteins were also revealed by Ponceau Red (PR). (**D**) Lines overexpressing RSH2-GFP and RSH3-GFP produced smaller seeds than wild type plants (** *P*<0.0001, Kruskal-Wallis test with *post hoc* Dunn test, n=254-1040). Error bars, SEM

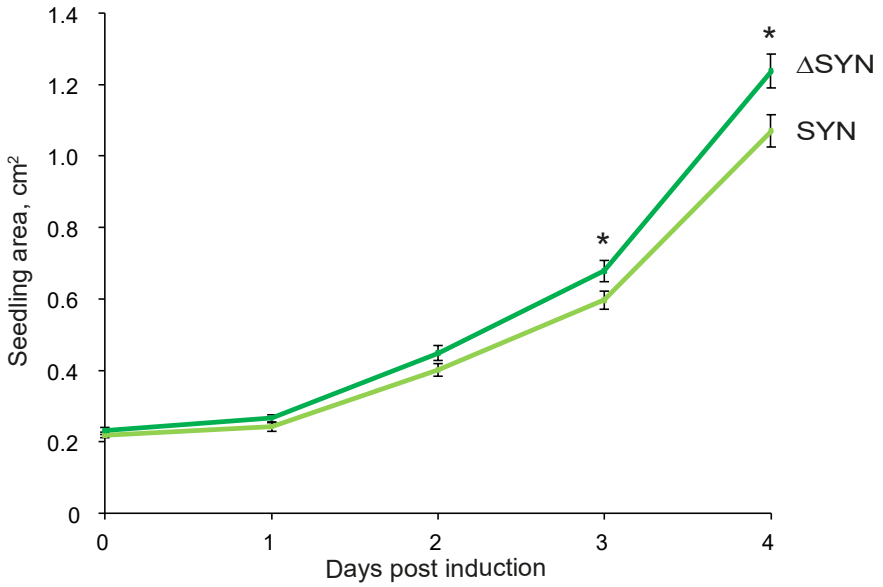

Supplemental Figure 4. Growth of SYN and ΔSYN following induction. 12 DAS seedlings were induced by submersion in 30 µM dexamethasone for 3 minutes and then photographed each day post induction for four days. Seedling area was determined in ImageJ. * *P*<0.05, two-way Student test, n=30 plants. Error bars, SEM.

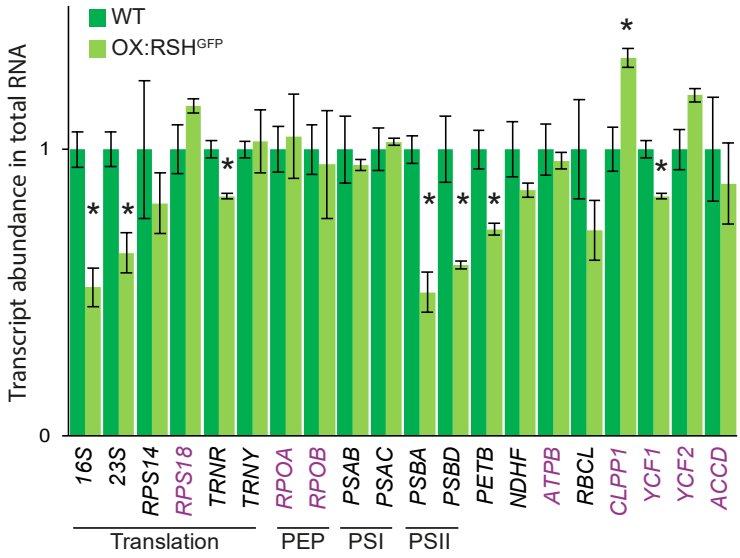

Supplemental Figure 5. qRT PCR analysis of plants overexpressing RSH3-GFP. qRT PCR for chloroplast transcripts in wildtype (dark green) and OX:RSH3-GFP.1 (OX:RSH3^{GFP}) seedlings (light green) 12 DAS. Data are presented as means ± SEM for three independent biological replicates and are normalized to *18S*, *APT1*, *PP2A* and *ULP7* reference transcripts. Transcripts produced principally or partially by NEP are indicated in purple. * *P*<0.05, two-way Student test.

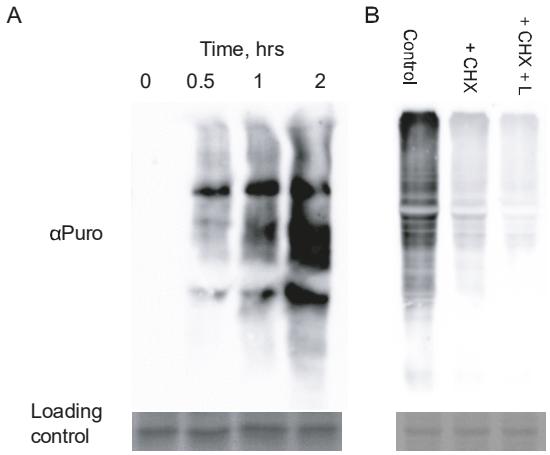

Supplemental Figure 6. Proof of concept for puromycin labeling in plants.
Puromycin is incorporated into cytosolic and chloroplastic proteins in a time dependent manner, and incorporation is inhibited by translation inhibitors. (**A**) Immunoblots of total Arabidopsis seedling proteins using a monoclonal anti-puromycin antibody (αPuro). 12-day old Arabidopsis seedlings were labeled with 50 µg/ml puromycin for the indicated time intervals before extraction of proteins, and equal quantities of protein were separated by SDS PAGE. Note the absence of a background signal in the unlabeled sample (0 hrs). (**B**) Immunoblots of equal quantities of chloroplast total protein from 12 day old seedlings labelled with puromycin for 1 hr. Incorporation of puromycin is inhibited by the pretreatment with the cytosolic translation inhibitor cycloheximide (CHX, 100 µg/ml) and is further inhibited by the chloroplast translation inhibitor lincomycin (L, 1 mM). Note that although cycloheximide blocks cytosolic translation, it also introduces a significant background signal that is caused by the puromycylation of cycloheximide arrested nascent peptide chains (David et al., 2012). This background is visible in the sample from seedlings treated with cycloheximide and lincomycin. Loading and transfer controls are RBCL stained with Ponceau red.

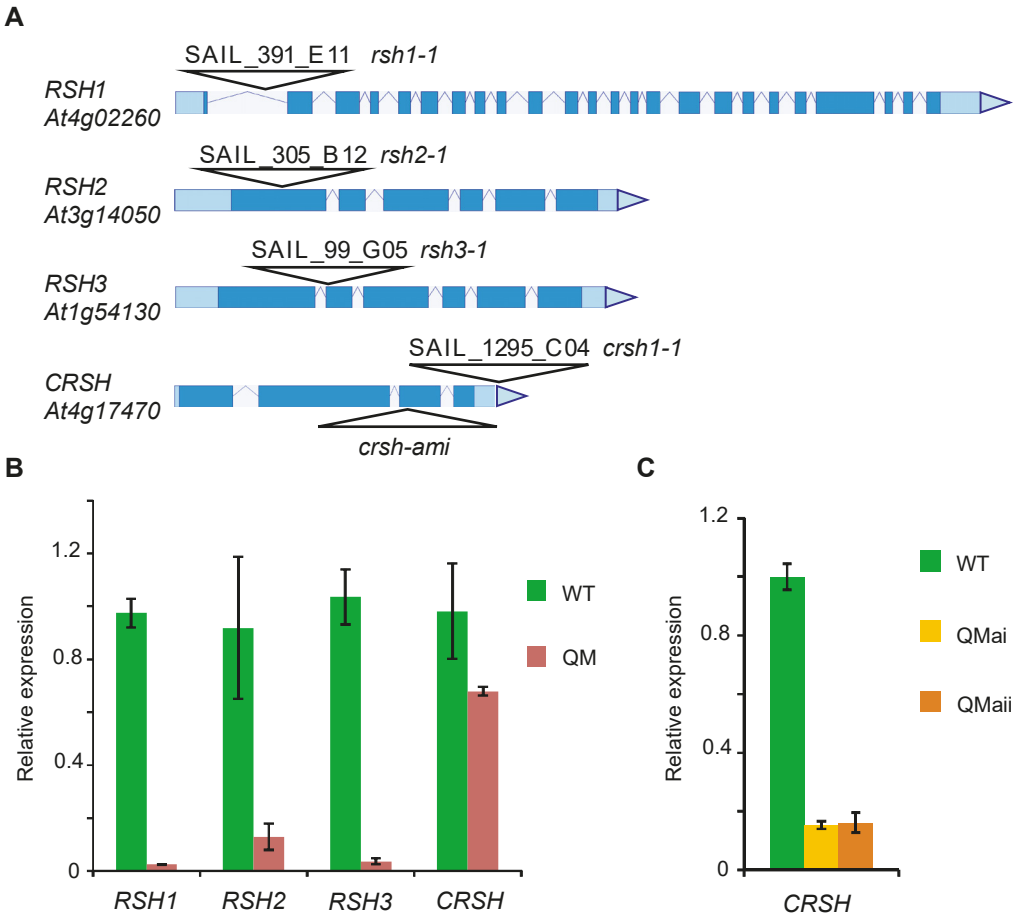

Supplemental Figure 7. Insertion sites and gene expression in the *RSH* mutants. (**A**) The insertion sites of the Arabidopsis TDNA insertion mutants used in this study. Insertions for *RSH1*, *RSH2* and *RSH3* are upstream of the conserved ppGpp synthase and hydrolase domains. The region of the *CRSH* transcript targeted by the amiRNA in *crsh-ami* is indicated. qRT PCR analysis of *RSH* gene expression in seedlings 12 DAS using primers downstream of the insertion sites in (**B**) the *rsh1-1 rsh2-1 rsh3-1 crsh1-1* quadruple mutant (QM) and (**C**) the *rsh1-1 rsh2-1 rsh3-1 crsh-ami* quadruple mutants (QMai and QMaii). QMai and QMaii have independent TDNA insertions for *crsh-ami*. Primers for qRT PCR and mutant genotyping are listed in Supplemental Data Set 1. qRT PCR data are presented as means ± SEM for three independent biological replicates and transcript abundance was normalized to *18S* and *PP2A* reference genes.

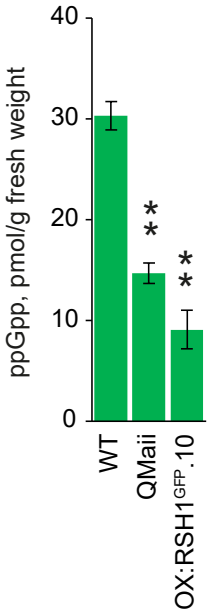

Supplemental Figure 8. ppGpp levels in QMaii and RSH1-GFP overexpressing plants were determined using a large scale extraction. ppGpp was extracted from seedlings grown on plates for 12 DAS and quantified by UPLC-MS, ** *P*<0.01, two-way Student t-test versus WT. Data are presented as means ± SEM for four independent biological replicates.

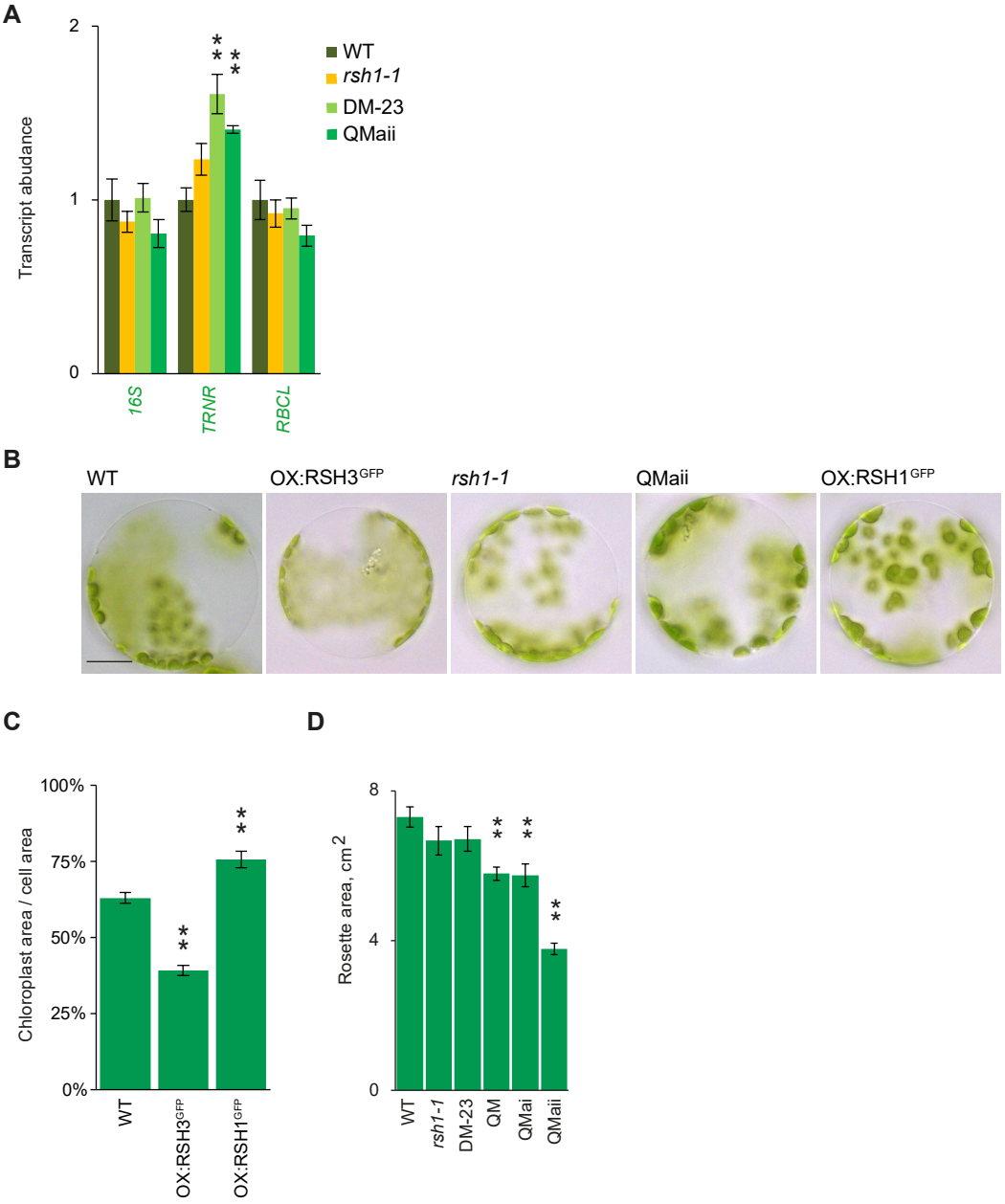

Supplementantal Figure 9. Phenotypes of *RSH* mutants during vegetative growth. (A) qRT PCR for chloroplast transcripts in wildtype and mutant plants 12 DAS. Data are presented as means ± SEM for five independent biological replicates and transcript abundance was normalized to *18S*, *APT1*, *PP2A* and *ULP7* reference transcripts. Statistical analysis was performed using ANOVA with *post hoc* Dunnett tests versus the wildtype control. (**B**) Images of representative protoplasts from fully expanded leaves of plants grown on soil at 35 DAS (scale bar, 20 µm). Analysis of these protoplast populations is presented in Figure 6B. (**C**) Chloroplast plan area per cell area was analyzed in intact mesophyll cells 28 DAS as described previously (Pyke and Leech, 1991). Data were analyzed by the Kruskal-Wallis test with the Dunn test *post hoc*, 44 cells were analyzed for WT, 50 for OX:RSH1-GFP.10 and 20 for OX:RSH3-GFP.1 (**D**) The average rosette area for selected mutants after 24 days growth on soil under long day conditions. Data were analyzed by ANOVA with *post hoc* Dunnett tests versus the wildtype controls, n=16 plants. OX:RSH3^{GFP}, OX:RSH3-GFP.1; OX:RSH1^{GFP}, OX:RSH1-GFP.10; ***P*<0.01; error bars, SEM.

Supplemental Figure 10. *RSH* mutants show visible growth phenotypes under short day conditions. After flowering under short day conditions *rsh1-1* plants rapidly become pale and show large numbers of senescent leaves compared to WT plants. In contrast, QMai and QMaii plants have small rosettes and darker leaves. The plants shown are 95 days old.

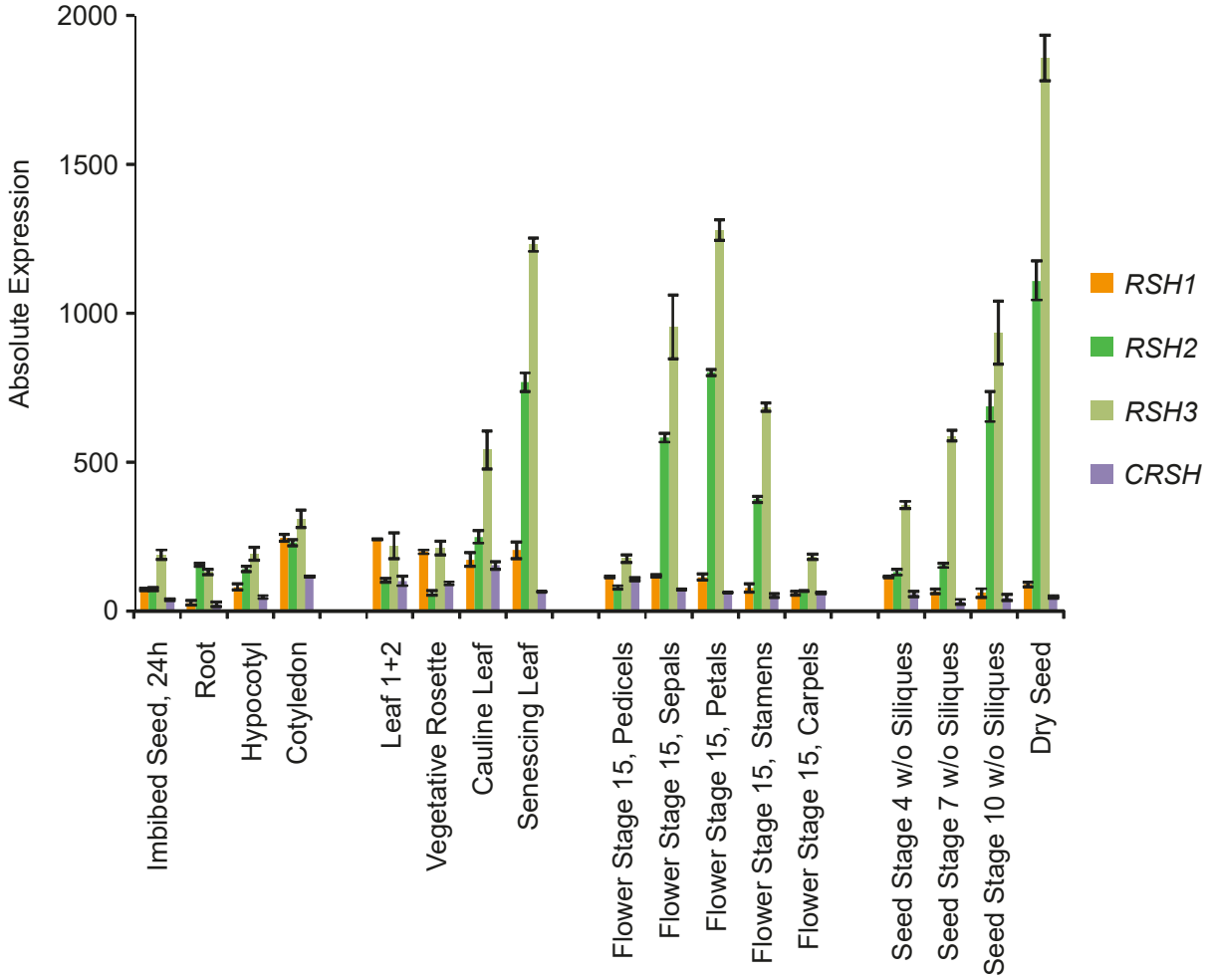

Supplemental Figure 11. *RSH2* and *RSH3* are strongly expressed during senescence and late plant development. Microarray expression profiles of Arabidopsis *RSH* genes (displayed from left to right: *RSH1*, *RSH2*, *RSH3* and *CRSH*) in different plant organs and at different stages of development. Data are presented as means ± SEM for three biological replicates. Data are from Schmid *et al.* (2005) and were retrieved from Genevestigator (Zimmermann *et al.*, 2004).

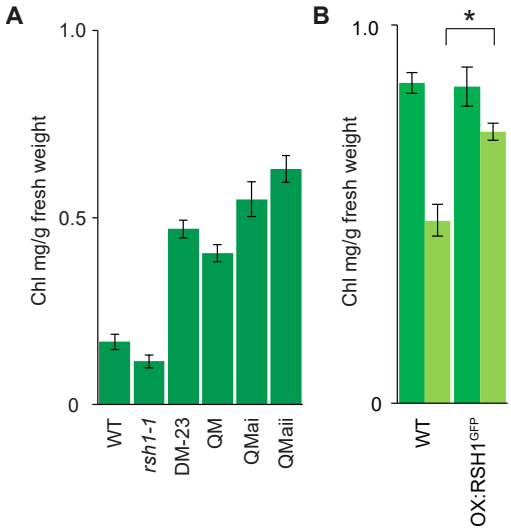

Supplemental Figure 12. Additional dark-induced senescence phenotypes. (**A**) *CRSH* may also contribute to the progression of dark-induced senescence. Chlorophyll levels in the leaves of wildtype and selected mutant lines following senescence induction. Prior to senescence induction plants used were grown under long day conditions for 30 days, and had just initiated flowering. This later developmental timepoint results in a faster progression of senescence than in Figure 7A. Chlorophyll loss was significantly greater in the wildtype than in DM-23, QM, QMai and QMaii (P<0.0001, n=3 plants). In addition the stay green phenotype of QMaii was significantly stronger than that of DM-23 suggesting that *CRSH* may also contribute during senescence despite its low level of expression, P<0.05. Data were analyzed by ANOVA. (**B**) Plants overexpressing RSH1-GFP show a stay-green phenotype. Chlorophyll content in 27 day old WT and OX:RSH1-GFP.10 (OX:RSH1^{GFP}) plants under normal growth conditions (dark green) or after senescence induction in the dark for three days (light green), * P = 0.01 WT versus OX:RSH1-GFP.10 after 3 days in the dark, n=3 plants, two-way Student t-test; error bars, SEM.

Supplemental Figure 13. Natural senescence is affected in *RSH* mutants. Leaves were recovered from the base of the rosette of 95 day old plants grown under short day conditions and arranged in order of age from the oldest on the left. Gaps were left for missing leaves. Natural senescence is visible in the wild type, and appears enhanced in *rsh1-1* and reduced in DM-23. QMaii leaves display an unusual senescence phenotype where they crumple and dry out while remaining green.

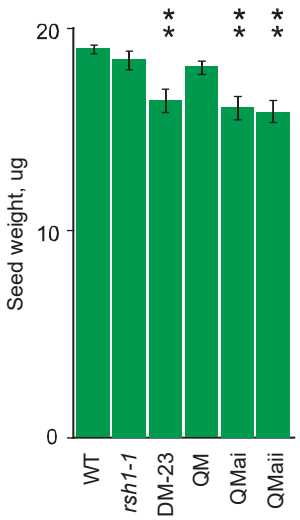

Supplemental Figure 14. *RSH* mutants have altered seed weight suggesting defects in nutrient remobilization or seed development. 300-500 seeds per plant were counted and weighed for seven or more biological replicates. Data were analyzed by ANOVA with *post hoc* Dunnett tests versus the wildtype controls, ***P*<0.001; error bars, SEM.

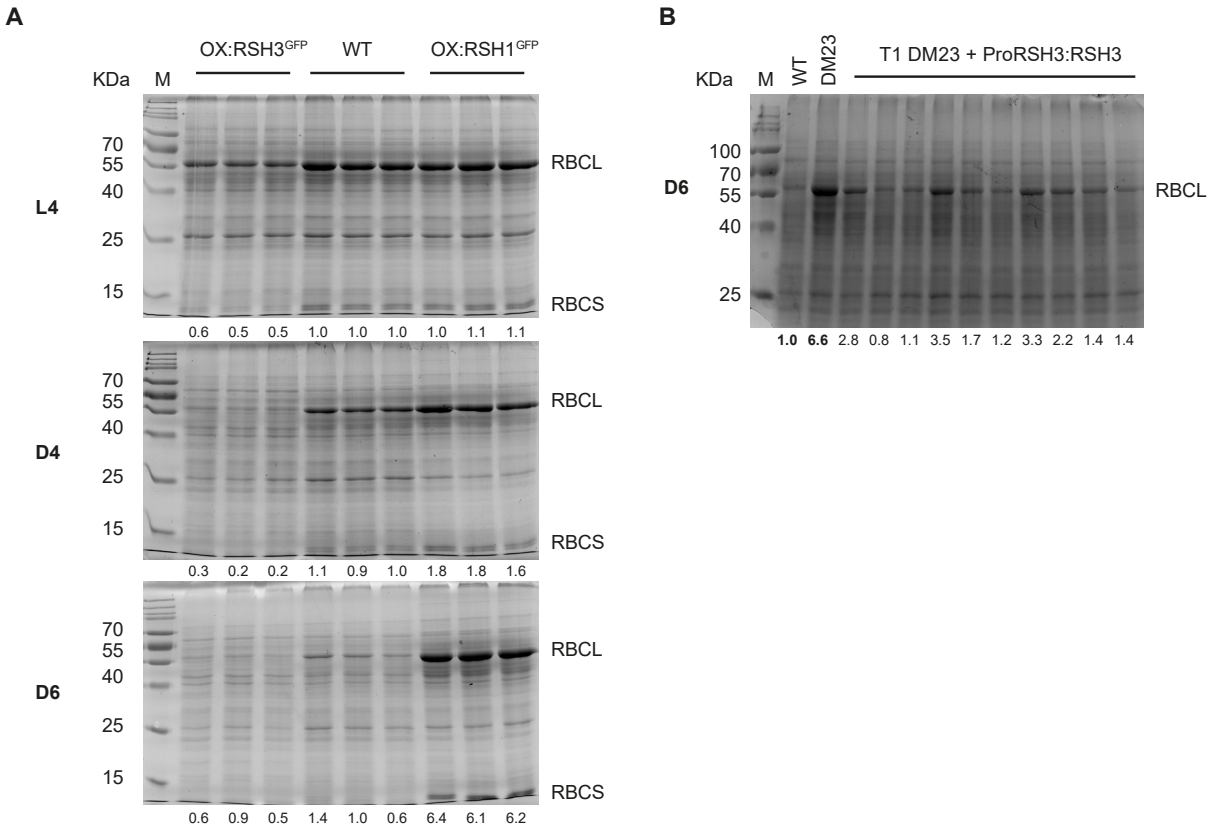

Supplemental Figure 15. RuBisCO degradation is regulated by ppGpp during dark-induced senescence. (**A**) Equal quantities of total protein from WT, OX:RSH3-GFP.1 (OX:RSH3^{GFP}) and OX:RSH1-GFP.10 (OX:RSH1^{GFP}) plants were separated by SDS-PAGE and visualized by Coomassie Brilliant Blue after extraction from the leaves of selected lines after 4 days (D4) and 6 days (D6) of darkness. Plants had grown for 21 DAS at the start of treatment. Non-treated leaves were used as a control on day 4 (L4). Extractions from the leaves of three independent plants are shown for each line. (**B**) The leaves of WT, DM-23 and independent first generation (T1) DM-23 lines transformed with the genomic *RSH3* (ProRSH3:RSH3) were analyzed as above after 6 days (D6) of darkness. Below each lane pixel densities for RBCL are shown, normalized to the wild type control on the same gel.

References

ATKINSON, G. C., TENSON, T. & HAURYLIUK, V. 2011. The RelA/SpoT homolog (RSH) superfamily: distribution and functional evolution of ppGpp synthetases and hydrolases across the tree of life. *PLoS One,* 6**,** e23479.

DAVID, A., DOLAN, B. P., HICKMAN, H. D., KNOWLTON, J. J., CLAVARINO, G., PIERRE, P., BENNINK, J. R. & YEWDELL, J. W. 2012. Nuclear translation visualized by ribosome-bound nascent chain puromycylation. *J Cell Biol,* 197**,** 45-57.

MIZUSAWA, K., MASUDA, S. & OHTA, H. 2008. Expression profiling of four RelA/SpoT-like proteins, homologues of bacterial stringent factors, in Arabidopsis thaliana. *Planta,* 228**,** 553-62.

PYKE, K. A. & LEECH, R. M. 1991. Rapid Image Analysis Screening Procedure for Identifying Chloroplast Number Mutants in Mesophyll Cells of Arabidopsis thaliana (L.) Heynh. *Plant Physiol,* 96**,** 1193-5.

SCHMID, M., DAVISON, T. S., HENZ, S. R., PAPE, U. J., DEMAR, M., VINGRON, M., SCHOLKOPF, B., WEIGEL, D. & LOHMANN, J. U. 2005. A gene expression map of Arabidopsis thaliana development. *Nat Genet,* 37**,** 501-6.

ZIMMERMANN, P., HIRSCH-HOFFMANN, M., HENNIG, L. & GRUISSEM, W. 2004. GENEVESTIGATOR. Arabidopsis microarray database and analysis toolbox. *Plant Physiol.,* 136**,** 2621-32.